Acta Biomaterialia 39 (2016) 180–191

Contents lists available at ScienceDirect

Acta Biomaterialia

journal homepage: www.elsevier.com/locate/actabiomat

Full length article

Diversity of multinucleated giant cells by microstructures of hydroxyapatite and plasma components in extraskeletal implantation model

Kota Morishita [a,b], Eri Tatsukawa [b], Yasuaki Shibata [b,1], Fumio Suehiro [c], Masanobu Kamitakahara [d], Taishi Yokoi [d,2], Koji Ioku [e], Masahiro Umeda [a], Masahiro Nishimura [c], Tohru Ikeda [b,*]

[a] Department of Clinical Oncology, Nagasaki University Graduate School of Biomedical Sciences, 1-7-1 Sakamoto, Nagasaki 852-8588, Japan
[b] Department of Oral Pathology and Bone Metabolism, Nagasaki University Graduate School of Biomedical Sciences, 1-7-1 Sakamoto, Nagasaki 852-8588, Japan
[c] Department of Prosthodontics, Kagoshima University Graduate School, 8-35-1 Sakuragaoka, Kagoshima 890-8544, Japan
[d] Graduate School of Environmental Studies, Tohoku University, 6-6-20 Aramaki, Aoba-ku, Sendai, Miyagi 980-8579, Japan
[e] Department of Chemistry, Faculty of Economics, Keio University, 4-4-1 Yokohama, Kanagawa 223-8521, Japan

ARTICLE INFO

Article history:
Received 5 February 2016
Received in revised form 15 April 2016
Accepted 2 May 2016
Available online 3 May 2016

Keywords:
Foreign body giant cell
Osteoclast
Hydroxyapatite
Microstructure
Cathepsin K

ABSTRACT

Foreign body giant cells (FBGCs) and osteoclasts are multinucleated giant cells (MNGCs), both of which are formed by the fusion of macrophage-derived mononuclear cells. Osteoclasts are distinct from FBGCs due to their bone resorption ability; however, not only morphological, but also functional similarities may exist between these cells. The characterization and diversity of FBGCs that appear in an *in vivo* foreign body reaction currently remain incomplete. In the present study, we investigated an *in vivo* foreign body reaction using an extraskeletal implantation model of hydroxyapatite (HA) with different microstructures. The implantation of HA granules in rat subcutaneous tissue induced a foreign body reaction that was accompanied by various MNGCs. HA granules composed of rod-shaped particles predominantly induced cathepsin K (CTSK)-positive FBGCs, whereas HA granules composed of globular-shaped particles predominantly induced CTSK-negative FBGCs. Plasma, which was used as the binder of ceramic granules, stimulated the induction of CTSK-positive FBGCs more strongly than purified fibrin. Furthermore, the implantation of HA composed of rod-shaped particles with plasma induced tartrate-resistant acid phosphatase (TRAP)-positive MNGCs in contrast to HA composed of globular-shaped particles with purified fibrin, which predominantly induced CTSK-negative and TRAP-negative typical FBGCs. These results suggest that CTSK-positive, TRAP-positive, and CTSK- and TRAP-negative MNGCs are induced in this subcutaneous implantation model in a manner that is dependent on the microstructure of HA and presence or absence of plasma.

Statement of Significance

We attempted to elucidate the mechanisms responsible for the foreign body reaction induced by the implantation of hydroxyapatite granules with different microstructures in rat subcutaneous tissue with or without plasma components as the binder of ceramic granules. By analyzing the expression of two reliable osteoclast markers, we detected tartrate-resistant acid phosphatase-positive multinucleated giant cells, cathepsin K-positive multinucleated giant cells, and tartrate-resistant acid phosphatase- and cathepsin K-negative multinucleated giant cells. The induction of tartrate-resistant acid phosphatase-positive multinucleated giant cells was plasma component-dependent while the induction of cathepsin K-positive multinucleated giant cells was influenced by the microstructure of hydroxyapatite. This is the first study to show the conditions dividing the three kinds of multinucleated giant cells in the foreign body reaction.

Abbreviations: FBGC, foreign body giant cell; MNGC, multinucleated giant cell; HA, hydroxyapatite; CTSK, cathepsin K; TRAP, tartrate-resistant acid phosphatase; MMP, matrix metalloproteinase; RANKL, receptor activator of nuclear factor kappa-B ligand; M-CSF, macrophage colony-stimulating factor; DC-STAMP, dendritic cell-specific transmembrane protein; IL, interleukin; GM-CSF, granulocyte-macrophage colony-stimulating factor.

* Corresponding author.
E-mail address: tohrupth@nagasaki-u.ac.jp (T. Ikeda).
[1] Present address: Department of Histology and Cell Biology, Nagasaki University Graduate School of Biomedical Sciences, 1-12-4 Sakamoto, Nagasaki 852-8523, Japan.
[2] Present address: Materials Research and Development Laboratory, Japan Fine Ceramics Center, 2-4-1 Mutsuno, Atsuta-ku, Nagoya 456-8587, Japan.

http://dx.doi.org/10.1016/j.actbio.2016.05.002
1742-7061/

1. Introduction

Foreign body giant cells (FBGCs) and osteoclasts are both multinucleated giant cells (MNGCs) generated by the fusion of mononuclear progenitor cells derived from a monocyte-macrophage lineage. Osteoclasts are easily distinguished from FBGCs due to their bone resorption ability [1]. Osteoclasts are one of the most important regulators of bone metabolism and are essential for maintaining the homeostasis of bone volume and calcium concentrations in serum. Osteoclasts dissolve bone mineral, chiefly composed of hydroxyapatite (HA) with acid synthesized by their acidification enzymes, such as carbonic anhydrase and proton ATPase [2]. Bone matrix proteins are chiefly digested by matrix metalloproteinase-9 (MMP-9) and cathepsin K (CTSK), both of which degrade collagen, the major component of the bone matrix. Hence, these enzymes are important markers for identifying osteoclasts [3–5]. Tartrate-resistant acid phosphatase (TRAP) and calcitonin receptors have also been identified as important markers of osteoclasts [6]. In the presence of macrophage colony-stimulating factor (M-CSF), osteoclasts are induced by the stimulation of receptor activator of nuclear factor kappa-B ligand (RANKL) through its receptor, RANK, which is expressed in mononuclear macrophages [7–9]. RANK binds with RANKL to stimulate the transcriptional factor NFATc1, which leads to the induction of multinucleated osteoclasts [10,11]. Therefore, RANK and NFATc1 are also important markers of osteoclasts [9]. Multinucleation is considered essential for bone resorption; however, the phenotype of mice deficient in the dendritic cell-specific transmembrane protein (DC-STAMP) or osteoclast stimulatory transmembrane protein (OC-STAMP), both of which are key molecules in cell fusion for the formation of MNGCs, revealed bones with bone marrow cavities in spite of almost no multinucleated osteoclasts existing [12,13]. These findings indicate that mononuclear preosteoclasts have the ability to resorb bone similar to multinucleated osteoclasts.

DC-STAMP- and OC-STAMP-deficient mice have a disorder for multinucleation of not only osteoclasts, but also FBGCs [12,13]. FBGCs have been classified into several groups based on their *in vivo* locations and morphological characteristics; however, the functional diversity of FBGC remains largely unclear. One of the reasons for the difficulties associated with analyzing FBGCs is that there are very limited numbers of useful specific markers to identify these cells [14–16]. FBGCs were previously shown to be induced *in vitro* by the stimulation of interleukin (IL)-4 and/or IL-13 in the presence of granulocyte-macrophage colony stimulating factor (GM-CSF) or M-CSF [17,18]. The biological significance of FBGCs and osteoclasts differs and previous studies also suggested that the biogenesis of FBGCs and osteoclasts are mutually exclusive [19–23]; however, part of the biological mechanism to form MNGCs is similar between these cell types [15].

We have been investigating the repair of bone defects implanted with ceramics using animal models. In the course of our research, HA composed of rod-shaped particles has been synthesized using an applied hydrothermal method [24,25]. HA synthesized with a hydrothermal process (HHA) and HA synthesized by conventional sintering (SHA) have been implanted into bone defects and the resulting biological responses were compared. Our findings showed that the number of osteoclasts was significantly larger in the region implanted with HHA than in that implanted with SHA. Furthermore, a significantly larger amount of bone was induced in the region implanted with HHA than in that implanted with SHA [26,27]. These findings suggest that HHA exhibits more potent osteoclast-homing activity than SHA, which results in the formation of a larger amount of bone in the implanted region. When implanted into bone defects, the calcium phosphate ceramics have been shown to be attached with osteoclasts and involved in the bone generated by osteoblasts [26–28]. This means that calcium phosphate ceramics tend to be recognized as bone equivalent materials rather than foreign bodies if they are surrounded by a large amount of bone. In the extraskeletal tissue, calcium phosphate ceramics are usually recognized by FBGCs as foreign bodies. When calcium phosphate ceramics are implanted into extraskeletal soft tissue, a foreign body reaction may also be influenced by their microstructures, and their microstructures may control certain phenotypes of FBGCs. However, information regarding this issue is still limited [29,30], and the implantation of calcium phosphate ceramics with different microstructures into extraskeletal soft tissue may contribute to examinations on the diversity of FBGCs. In addition, it was suggested that mononuclear osteoclast precursor cells circulate in the blood stream and settle on the surface of bone tissue [31], and HHA and/or SHA may act as scaffolds of osteoclast precursor cells and osteoclast-like MNGCs may be detected on the surface of these implants. In the present study, we implanted HHA and SHA granules into rat subcutaneous tissue and compared foreign body reactions in order to evaluate whether the microstructure of HA influences the phenotype of FBGCs around these implants.

2. Materials and methods

2.1. Preparation of ceramic granules

A total of 13.5 g of α-TCP powder (Taihei Chemical Ind. Co., Ltd., Osaka, Japan) was mixed and kneaded with 67.5 g of 10% gelatin solution, and dropped into a stirred oil bath heated to 80 °C. The bath was then chilled on iced water and spherical α-TCP/gelatin granules were formed. The granules were separated from the oil,

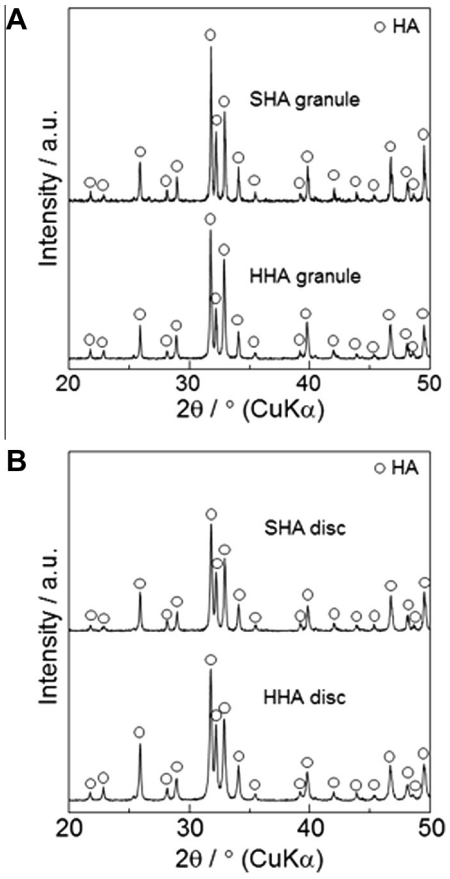

Fig. 1. X-ray diffractometry of HHA and SHA granules and discs used in this study.

rinsed, and then heated at 1200 °C for 30 min to remove gelatin and maintain the crystal phase of α-TCP. The α-TCP granules formed were sieved and granules 0.5–0.6 mm in diameter were used in experiments. A total of 0.2 g of the obtained α-TCP granules was set in a polytetrafluoroethylene-lined autoclave with 20 ml of water and maintained at 160 °C under saturated water vapor pressure for 20 h as a hydrothermal treatment. In order to complete the formation of HA, 0.2 g of the resultant granules were hydrothermally treated again in 20 ml of ammonia solution at pH 11 at 105 °C for 3 h to obtain spherical HHA granules.

Spherical SHA granules were prepared as follows. Ten grams of HA powder (Ube Material Industries, Ltd., Ube, Japan) was mixed and kneaded with 50 g of 10% gelatin solution, and then dropped into a stirred oil bath chilled to 5 °C. The granules were separated from the oil, rinsed, and heated at 1000 °C for 2 h to remove gelatin and sinter. The SHA granules obtained were sieved and granules 0.5–0.6 mm in diameter were used for experiments.

Synthesized HHA and SHA granules were analyzed by powder X-ray diffractometry with graphite-monochromatized CuKα radiation (XRD; RINT-2200VL, Rigaku, Tokyo, Japan). We confirmed that the main phases of HHA and SHA were HA (Fig. 1A). The rod-shaped particles of spherical HHA granules (Fig. 2A) and globular-shaped particles of spherical SHA granules (Fig. 2D) were confirmed using a scanning electron microscope (SEM; SU8000, Hitachi, Ltd., Tokyo, Japan) (Fig. 2B, E). The width of the rod-shaped particles of HHA granules was 0.30 ± 0.12 μm (n = 100), while their length was about 10 μm. It was difficult to obtain the exact length because the rod-shaped particles were hidden by other particles and inclined. The size of the globular-shaped particles of SHA granules was 0.28 ± 0.09 μm in diameter (n = 100) assuming that the particles were separated spheres. The specific surface areas of the HHA and SHA granules measured by Brunauer-Emmett-Teller (BET) method using N_2 gas with a gas sorption analyzer (Autosorb-iQ, Quantachrome Instruments, Boynton Beach, FL) were 5 and 2 m^2/g, respectively.

2.2. Preparation of ceramic discs

HHA discs were prepared using the following method. A total of 0.3 g of α-TCP powder was inserted into a mold 12 mm in diameter and pressed at 200 MPa. The α-TCP discs obtained were set in a polytetrafluoroethylene-lined autoclave with 20 ml of water and maintained at 160 °C under saturated water vapor pressure for 20 h as a hydrothermal treatment. In order to complete the formation of HA, the resultant discs were hydrothermally treated again in 20 ml of ammonia solution at pH 11 at 105 °C for 3 h. They were then rinsed and dried at 90 °C. SHA discs were prepared using the following method. A total of 0.3 g of HA powder was inserted into a mold 14 mm in diameter and pressed at 200 MPa. It was heated at 900 °C for 2 h for sintering.

Synthesized HHA and SHA granules were analyzed by powder X-ray diffractometry as described above, and the main phases of HHA and SHA were HA (Fig. 1B). The rod-shaped particles of HHA discs and globular-shaped particles of SHA discs were confirmed

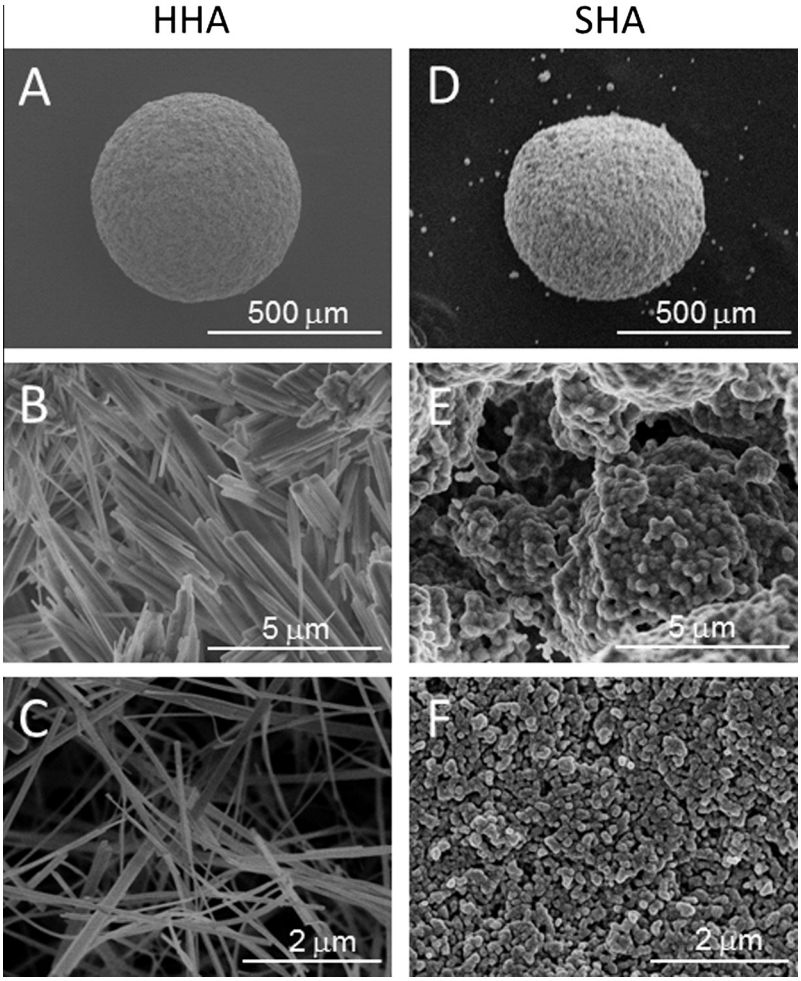

Fig. 2. Scanning electron micrographs of an overview (A, D) and the microstructure (B, E) of HHA (A, B) and SHA (D, E) granules, and the microstructure of HHA (C) and SHA (F) discs.

using a scanning electron microscope (SU8000, Hitachi, Ltd., Tokyo, Japan) (Fig. 2C, F).

2.3. Animals and operative procedures

Forty milligrams of ceramic granules was placed into a 1.5-ml microcentrifuge tube. Ceramic granules were then soaked in 20 μl of Bolheal® (Kaketsuken, Kumamoto, Japan), which was made from human fibrinogen and gelled with thrombin following the manufacturer's protocol. In other experiments, 100 μl of 4-week-old male F344 rat plasma prepared from frozen stock was added. Plasma in each tube was gelled by the addition of 5 μl of 3.3% calcium chloride and centrifugation.

Sixteen male 10-week-old F344 rats were anesthetized with an intraperitoneal injection of ketamine (40 mg/kg body weight) and xylazine (3 mg/kg body weight) prior to surgery. These gels were implanted into the back subcutaneous tissue of the anesthetized F344 rats. The gels were implanted into two portions on the back of each rat. Four implantations were performed for each group in these experiments. Rats were euthanized four and 12 weeks after implantation. Implanted granules were extracted with the surrounding subcutaneous tissue and fixed with 4% paraformaldehyde in 0.1 M phosphate buffer (pH 7.2) at 4 °C for 24 h. After fixation, each specimen was cut in half with a razor, with one being provided for undecalcified sections and the other for decalcified sections. Animal rearing and experiments were performed at the Biomedical Research Center, Center for Frontier Life Sciences, Nagasaki University, following the Guidelines for Animal Experimentation of Nagasaki University (Approval no. 1112190960) under specific pathogen-free conditions.

2.4. Histological procedures

Regarding undecalcified sections, fixed specimens were dehydrated and embedded in 2-hydroxyethyl methacrylate/methyl methacrylate/2-hydroxyethyl acrylate mixed resin (all from Wako Pure Chemical, Osaka, Japan) and sectioned at a thickness of 3 μm using a LEICA RM2155 microtome (Leica, Nussloch, Germany). These sections were stained with Giemsa's azur eosin methylene blue solution (Merck, Darmstadt, Germany) or histochemically stained for TRAP activity. Staining for TRAP activity was performed using naphthol AS-MX phosphate (Sigma-Aldrich, St. Louis, MO) as

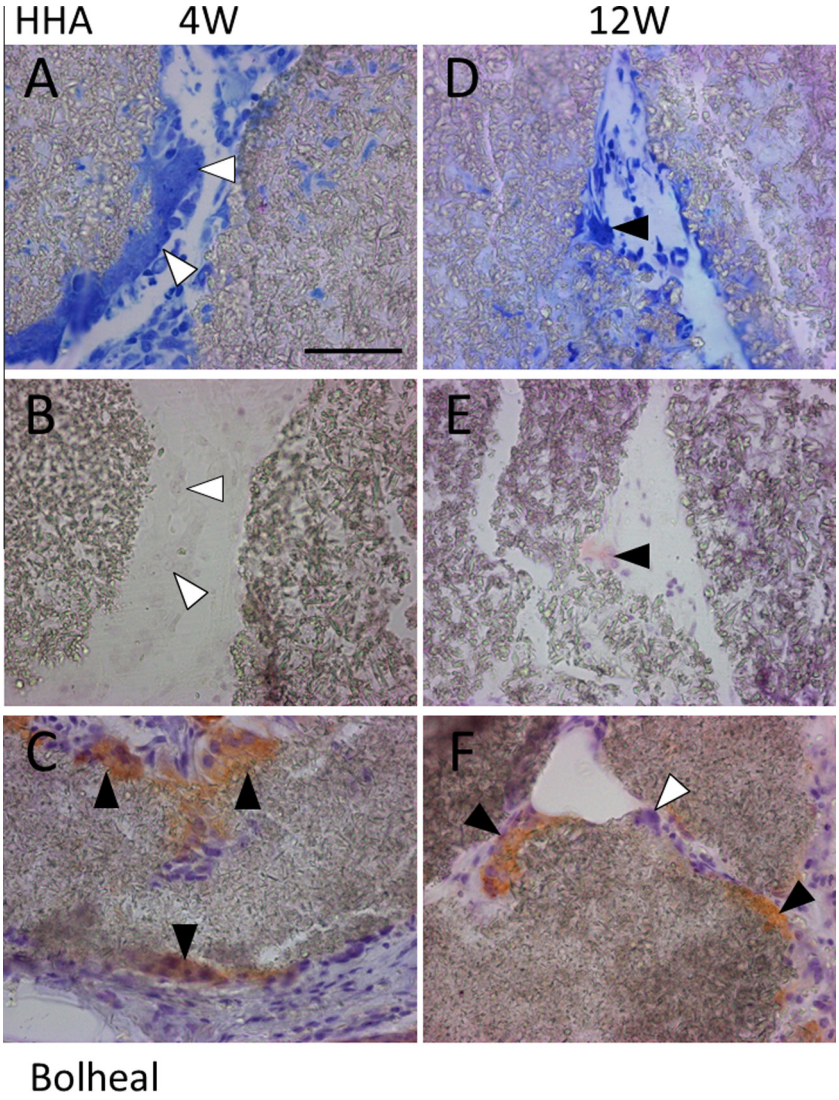

Fig. 3. Histological views of specimens implanted with HHA granules bound with Bolheal®. Sections 4 weeks after implantation (A–C) and 12 weeks after implantation (D–F) stained with Giemsa's solution (A, D), the histochemical detection of TRAP activity (B, E), and immunohistochemical detection of CTSK (C, F). Arrowheads represent MNGCs with (black arrowheads) and without (white arrowheads) TRAP activity (A, B, D, E). Most MNGCs showed the brown chromogenic reaction of anti-CTSK antibody binding (C, F). Arrowheads represent MNGCs with (black arrowheads) and without (white arrowheads) CTSK antibody binding. The scale bar represents 50 μm.

a substrate, fast red RC salt (Sigma-Aldrich) as a coupler and 0.05 M sodium tartrate in 0.05 M acetic acid buffer (pH 5). Regarding decalcified sections, fixed specimens were decalcified in 0.5 M ethylenediamine tetraacetic acid (EDTA) solution at 4 °C with gentle agitation. The decalcified samples were post-fixed with the fixative, dehydrated, embedded in paraffin, and 3-μm-thick sections were made and provided for further immunohistochemical analyses. The sections were placed in an autoclave at 121 °C for 15 min in 10 mM citrate buffer (DAKO, Carpinteria, CA) and incubated with a CTSK rabbit anti-rat polyclonal antibody (LifeSpan BioSciences, Seattle, WA) at 4 °C overnight. Immunohistochemical reactions were performed using the EnVision+ system (DAKO) following the manufacturer's protocol. Sections were counterstained with Meyer's hematoxylin.

2.5. In vitro analyses

Mouse bone marrow macrophages prepared from the femora and tibiae of 5-week-old female ddY mice (Japan SLC, Shizuoka, Japan) were expanded *in vitro* in minimum essential medium alpha supplemented with 10% fetal bovine serum, penicillin-streptomycin-glutamine (Life Technologies, Carlsbad, CA), and 30 ng/ml M-CSF (Sigma-Aldrich). Synthesized ceramic discs were inserted into 24-well type wells and macrophages (1×10^4 cells/cm^2) were plated on ceramic discs and cultured. As a control, macrophages were plated in wells without ceramic discs. After 6 days, the medium was removed and cells were histochemically stained for TRAP activity as described above. To evaluate multinucleation of macrophages, other sample sets were stained with DAPI (Dojindo Lab., Kumamoto, Japan) to detect cell nuclei and Acti-stain™ 488 (Cytoskeleton, Inc., Denver, CO.) to detect cytoplasmic actin fibers. These cells were analyzed using the ECLIPSE LV100D industrial microscope equipped with the INTENSILIGHT C-HGFI epifluorescence illuminator, filter blocks B-2A and DAPI and the DS-Ri1-U2 digital camera system (all from Nikon, Tokyo, Japan). For real-time PCR analysis, cells of the other sample sets were lysed with TRIzol® reagents (Life Technologies) to extract total RNA. After DNase treatment, cDNA was synthesized from total RNA with a ReverTra Ace (Toyobo, Osaka, Japan) reverse transcriptase. Real-time PCR was performed using Premix Ex Taq [Perfect Real Time] and the Thermal Cycler Dice Real Time System Lite (both from Takara, Shiga, Japan) with the following primers: glyceraldehyde-3-phosphate dehydrogenase (GPDH): Mm99999915_g1, TRAP: Mm00475698_m1, CTSK: Mm00484039_m1, NFATc1: Mm00479445_m1, c-Fms: Mm01266652_m1, RANK: Mm00437132_m1, carbonic anhydrase 2 (Car2): Mm00501576_m1 (all from Applied

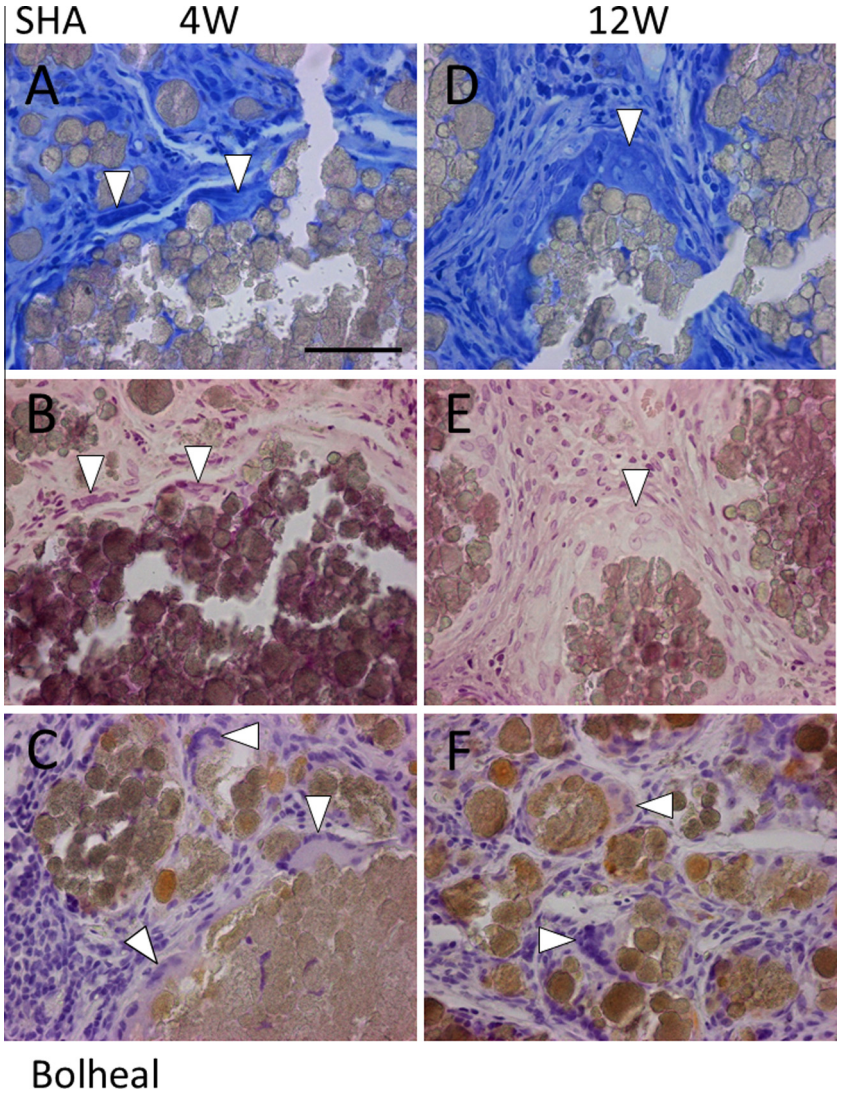

Fig. 4. Histological views of specimens implanted with SHA granules bound with Bolheal®. Sections 4 weeks after implantation (A–C) and 12 weeks after implantation (D–F) stained with Giemsa's solution (A, D), the histochemical detection of TRAP activity (B, E), and immunohistochemical detection of CTSK (C, F). White arrowheads represent MNGCs without TRAP activity (A, B, D, E). No MNGC showed the chromogenic reaction of anti-CTSK antibody binding (C, F, white arrowheads). The scale bar represents 50 μm.

BioSystems, Waltham, MA). The expression levels of each mRNA were normalized to the relative quantity of GPDH mRNA expressed in each sample. Data were statistically evaluated using the *t*-test with data from 3 identical experiments, and a *P* value <0.05 was considered significant.

3. Results

3.1. Histological analysis

TRAP-positive MNGCs were analyzed in plastic-embedded undecalcified sections using a histochemical procedure. TRAP-positive MNGCs (Fig. 3D, E, black arrowheads) and TRAP-negative MNGCs (Fig. 3A, B, white arrowheads) were both detected in specimens implanted with HHA granules bound with Bolheal®, which was made from purified human fibrin, whereas very few TRAP-positive MNGCs were observed in either specimen 4 or 12 weeks after implantation. CTSK-positive MNGCs were analyzed in paraffin-embedded decalcified sections using an immunohistochemical procedure. Most MNGCs on the surface of HHA granules bound with Bolheal® were CTSK-positive (Fig. 3C, F). In specimens implanted with SHA granules bound with Bolheal®, most MNGCs were negative for TRAP activity (Fig. 4A, B, D, E, white arrowheads) and CTSK (Fig. 4C, F, white arrowheads) 4 and 12 weeks after implantation.

In order to evaluate the effects of blood components, we analyzed specimens implanted with ceramic granules bound with plasma. Fewer MNGCs were detected on the surface of the HHA granules 4 weeks after the implantation of HHA granules bound with plasma than 12 weeks after implantation (Fig. 5A, D, arrowheads). TRAP-positive MNGCs (Fig. 5B, D, E, black arrowheads) and TRAP-negative MNGCs (Fig. 5A, B, D, E, white arrowheads) were both identified. Most MNGCs on the surface of HHA granules were CTSK-positive 4 and 12 weeks after implantation. Larger numbers of CTSK-positive MNGCs were detected in specimens 12 weeks after implantation than 4 weeks after implantation (Fig. 5C, F).

In the specimen implanted with SHA granules bound with plasma, MNGCs were present on the surface of SHA granules; however, the number of TRAP-positive MNGCs was very small 4 and 12 weeks after implantation (Fig. 6A, B, D, E, white arrow-

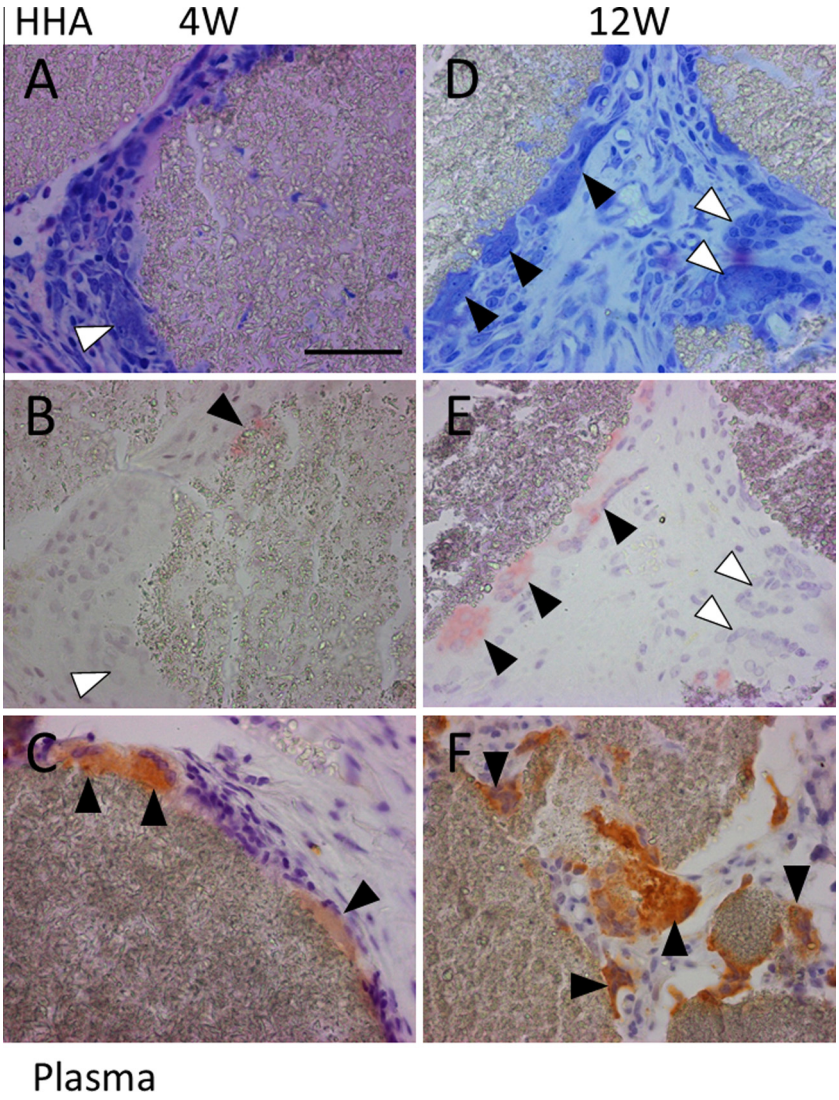

Fig. 5. Histological views of specimens implanted with HHA granules bound with plasma. Sections 4 weeks after implantation (A–C) and 12 weeks after implantation (D–F) stained with Giemsa's solution (A, D), the histochemical detection of TRAP activity (B, E), and immunohistochemical detection of CTSK (C, F). Arrowheads represent MNGCs with (black arrowheads) and without (white arrowheads) TRAP activity (A, B, D, E). Most MNGCs showed the brown chromogenic reaction of anti-CTSK antibody binding (C, F, black arrowheads). The scale bar represents 50 μm.

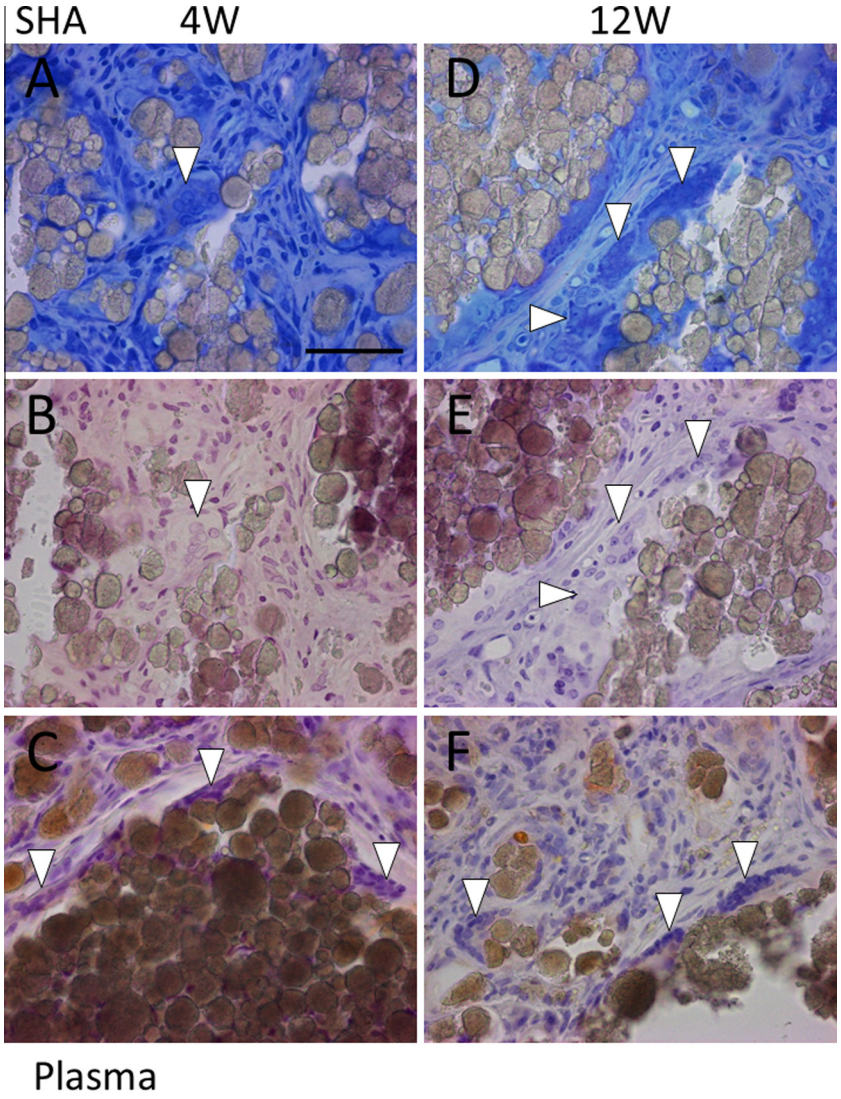

Fig. 6. Histological views of specimens implanted with SHA granules bound with plasma. Sections 4 weeks after implantation (A–C) and 12 weeks after implantation (D–F) stained with Giemsa's solution (A, D), the histochemical detection of TRAP activity (B, E), and immunohistochemical detection of CTSK (C, F). White arrowheads represent MNGCs without TRAP activity (A, B, D, E). No MNGC showed the chromogenic reaction of anti-CTSK antibody binding (C, F, white arrowheads). The scale bar represents 50 μm.

heads). In contrast to the specimens implanted with HHA granules, most MNGCs on the surface of SHA granules were negative for CTSK (Fig. 6C, F, white arrowheads).

The quantitation of TRAP-positive and CTSK-positive MNGCs is represented in Fig. 7. The number of TRAP-positive MNGCs was significantly larger in the specimen implanted with plasma as the binder of ceramic granules than in that implanted with Bolheal® as the binder of ceramic granules for both HHA and SHA (Fig. 7B). No significant difference was observed in the number of TRAP-positive MNGCs between specimens implanted with HHA and SHA granules (Fig. 7A) and between specimens 4 weeks and 12 weeks after implantation (Fig. 7C). The number of CTSK-positive MNGCs was significantly larger in the specimen implanted with HHA granules than in that implanted with SHA granules irrespective of the binder (Fig. 7D). Twelve weeks after implantation, the number of CTSK-positive MNGCs was significantly larger in the specimen implanted with plasma than in that implanted with Bolheal® for both HHA and SHA granules (Fig. 7E). In specimens implanted with plasma, the number of CTSK-positive MNGCs was significantly larger 12 weeks after implantation than 4 weeks after implantation for both HHA and SHA granules (Fig. 7F). Results are summarized in Fig. 8.

3.2. In vitro analyses

In order to evaluate whether HHA and SHA had a potential to differentiate macrophages into osteoclast progenitors without RANKL stimulation *in vitro*, the expression of osteoclast markers was compared among macrophages cultured on HHA discs, SHA discs, and plastic dishes. Few TRAP-positive cells were detected by the histochemical analysis (Fig. 9A, C). Multinucleation of macrophages was also rarely detected under the fluorescence microscope (Fig. 9B, D). In real-time PCR analysis, the expression of TRAP was significantly stronger in macrophages cultured on HHA and SHA discs than in those cultured on plastic dishes (Fig. 10A). The expression of CTSK was significantly stronger in macrophages cultured on HHA discs than in those cultured on SHA discs and plastic dishes (Fig. 10B). The expression of Car2 was significantly stronger in macrophages cultured on SHA discs and had strong tendency to be increased in those cultured on HHA discs compared to those cultured on plastic dishes (Fig. 10C). No significant differences were observed in the expression of NFATc1 or RANK (Fig. 10D, E). The expression of c-Fms was significantly lower in macrophages cultured on HHA discs and SHA discs than in those cultured on plastic dishes (Fig. 10F).

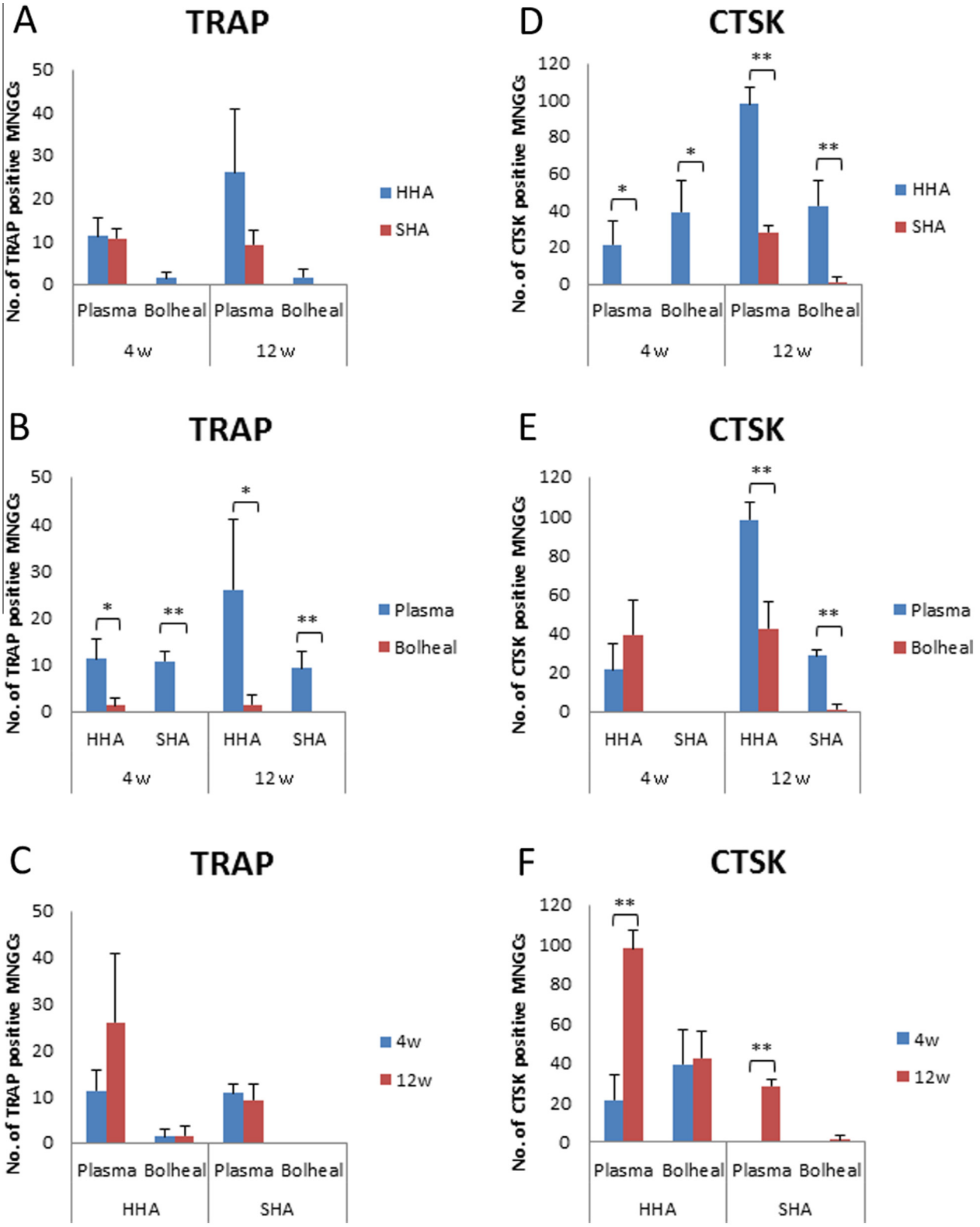

Fig. 7. Quantitation of TRAP-positive and CTSK-positive MNGCs in specimens implanted with HHA or SHA granules bound with plasma or Bolheal® evaluated with differences in the ceramic (A, D), differences in the binder (B, E), and differences in the term of implantation (C, F). $^{*}P < 0.05$, $^{**}P < 0.01$.

4. Discussion

Osteoclasts are specifically distributed on the surface of bone. However, the biological mechanisms underlying the bone-specific distribution of osteoclasts have not yet been elucidated in detail. In contrast to osteoclasts, FBGCs appear around foreign bodies, which include foreign materials, the caseous necrosis of tuberculosis, cholesterol deposition, and keratin. Due to the highly specific distribution of osteoclasts versus the non-specific distribution of FBGCs and the difference in each precursor cell, osteoclasts and

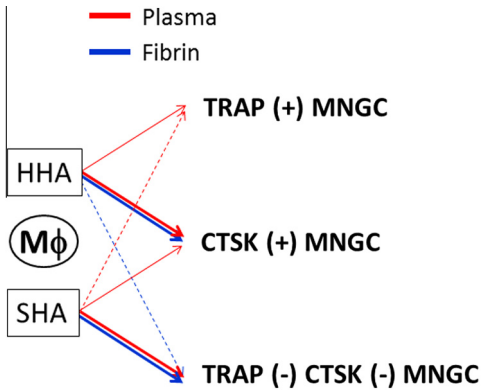

Fig. 8. Summary of emersion of MNGCs.

FBGCs are regarded as completely different MNGCs. However, difficulties are associated with identifying specific differentiation markers with the ability to distinguish between osteoclasts and FBGCs. Although TRAP, CTSK, and MMP-9 are reliable markers of cells in the osteoclast lineage, several studies showed that some of these markers were expressed in FBGCs under certain conditions [32–34]. In addition, a recent study demonstrated that FBGCs had the ability to dissolve calcium phosphate ceramic, similar to osteoclasts, but were unable to resorb bone [35]. These findings indicate that FBGCs also possess the potential for acidification to dissolve bone minerals and strongly suggest that there are certain functional diversities in FBGCs, some of which possess similar characteristics to osteoclasts.

In the present study, the induction of CTSK activity in FBGCs depended on the microstructure of HA and plasma. We previously showed that the affinity of serum proteins differed between HHA and SHA by analyzing the profiles of serum proteins adsorbed to these ceramics, and vitamin D-binding protein preferentially adsorbed to HHA was suggested to be associated with potent osteoclast-homing activity from the data that its deglycosylated active form, macrophage activating factor, stimulated RANKL-induced osteoclastogenesis [36]. Our previous findings indicate that serum proteins with high affinity to HHA, especially vitamin D-binding protein, may contribute to the induction of CTSK-positive FBGCs. Most FBGCs on the surface of HHA were CTSK-positive. Therefore, a significantly larger number of FBGCs were induced with plasma than with Bolheal®, suggesting that certain serum proteins with high affinity to HHA contributed to the induction of CTSK-positive FBGCs.

As reported previously, the microstructure of ceramics may directly influence cell differentiation [29,30]. In the present study, a large number of FBGCs on the surface of SHA were negative for TRAP and CTSK activity irrespective of the binder. Hence, the microstructure of HA may also be directly associated with the induction of CTSK-positive FBGCs. An *in vitro* analysis showed that neither HHA nor SHA had the potential to induce osteoclasts or MNGCs from macrophages. This may be caused partly by differences between the *in vivo* and *in vitro* conditions or limitations of the culture period of the *in vitro* experiments, but PCR analysis revealed that the expression of TRAP and CTSK was significantly higher in macrophages cultured on HHA or SHA discs than in those cultured on plastic dishes. In addition, the expression of CTSK was significantly stronger in macrophages cultured on HHA discs than in those cultured on SHA discs. These *in vitro* results support the hypothesis that the microstructure of HA directly contributes to the induction of CTSK-positive FBGCs in subcutaneous tissue. The absence of a significant difference in the expression of NFATc1 among these macrophages suggests that the alteration observed in the expression of TRAP, CTSK and Car2 was independent of the mechanism responsible for osteoclast differentiation.

TRAP-positive MNGCs were also detected in the present study. Most MNGCs on the surface of HHA granules were positive for CTSK, indicating that some TRAP and CTSK double-positive MNGCs were present. We did not perform an electron microscopic analysis to detect ruffled borders, the most definite marker of osteoclasts to date [2,35], and whether TRAP-positive MNGCs are identical to osteoclasts currently remains unclear. We have been investigating

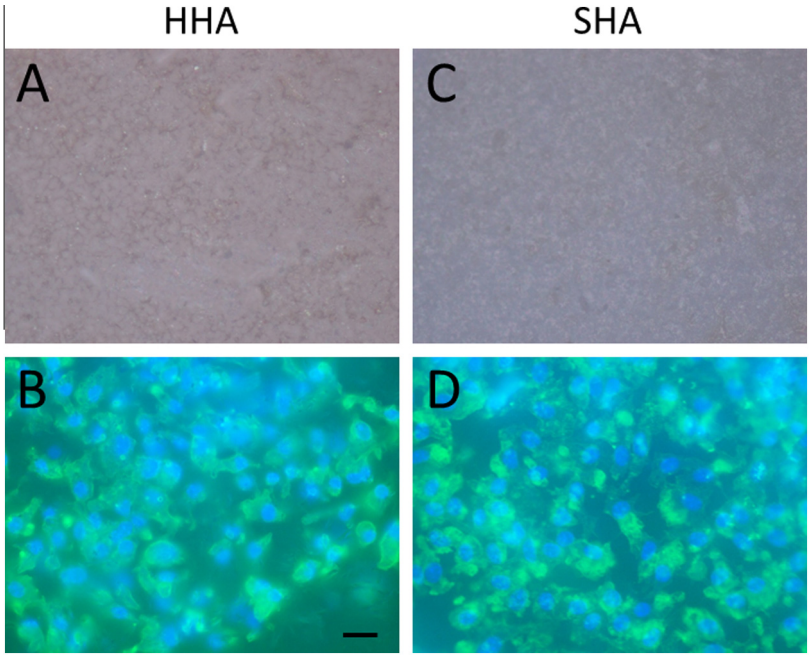

Fig. 9. Evaluation of TRAP activity and multinucleation of macrophages cultured on HHA and SHA discs. Representative views of macrophages cultured on HHA discs (A, B) and SHA discs (C, D) after histochemical staining of TRAP activity (A, C) and fluorescence microscopy to detect nuclei with DAPI and cytoplasmic actin fibers with Acti-stain™. The scale bar represents 10 μm.

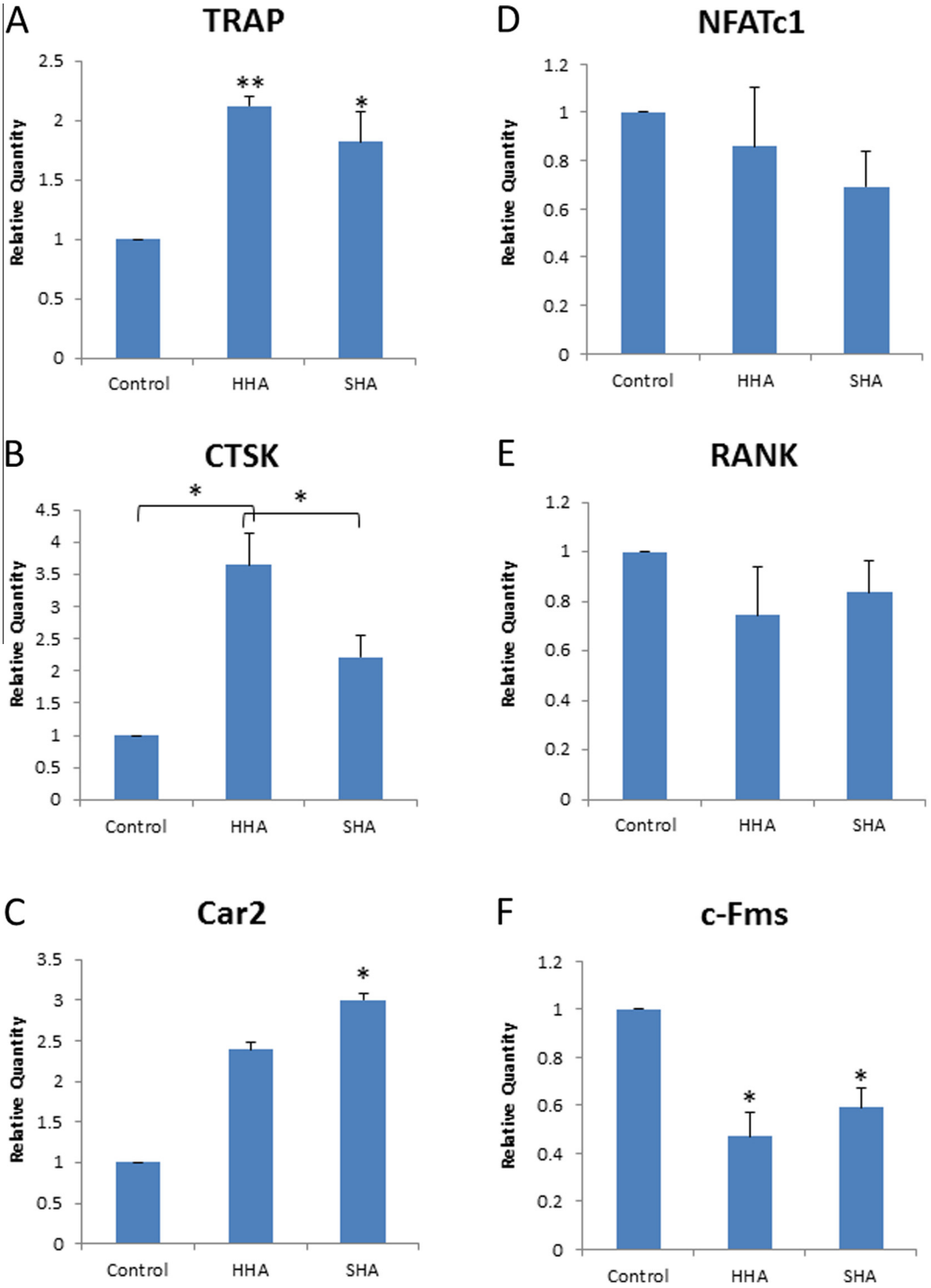

Fig. 10. A real-time PCR analysis for the relative mRNA expression of osteoclast markers in macrophages cultured for 6 d on HHA discs, SHA discs, or plastic dishes (Control). $^{*}P < 0.05$.

the healing of bone defects with the implantation of HA or β-TCP, and have found that all MNGCs in the implanted region exhibited TRAP activity, that MNGCs on the surface of implants were indistinguishable from osteoclasts on the surface of newly formed bone, and also that hybrid trabeculae composed of bone and ceramics formed [28,37]. Hence, we suggest that HA and β-TCP are recognized in bone tissue as bone equivalent materials rather than foreign bodies, and are involved in physiological bone metabolism. It is also true that granulomatous reactions occur around dental implants [38,39]. In our previous studies, we created bone defects in the metaphysis of the femur of relatively young rats [26,27,37]. These discrepancies may be caused by differences in osteogenic activity or inflammatory reactions, which tend to occur around dental implants [40]. In this study, we used an extraskeletal model

for analyzing *in vivo* conditions of osteoclastogenesis and formation of FBGCs to exclude the influence of bone tissue accompanied with osteoclasts and RANKL-expressing osteoblasts. However, there may be some limitations in analyzing exact tissue reactions for these ceramics as bone substitutes in the bone and further analysis may be necessary using older animals or bone marrow stromal cells. Our previous findings indicate that TRAP and CTSK double-positive MNGCs may be osteoclasts. However, the limited number of TRAP-positive MNGCs observed suggests that even if some TRAP-positive MNGCs are identical to osteoclasts, the osteoclast-homing activity of HA is not high and RANKL-expressing osteoblasts are needed for osteoclastogenesis.

The induction of TRAP-positive MNGCs was associated with plasma rather than the microstructure of HA. These results suggest that certain plasma components contribute to the induction of TRAP-positive MNGCs in subcutaneous tissue. Takahashi's group previously reported that a large number of osteoclasts were generated from RANK-positive osteoclast precursor cells, which circulated in the bloodstream. They also showed that osteoclast precursor cells settled on the surface of bone and differentiated into preosteoclasts in contact with RANKL, the transmembrane ligand of RANK synthesized by osteoblasts, and that mononuclear preosteoclasts fused with one another to form multinucleated osteoclasts [31]. Considering these hypotheses, HA may have the potential to settle osteoclast precursor cells. The expression of c-Fms was significantly lower in macrophages cultured on HHA or SHA discs than in those cultured on plastic dishes. In contrast, the expression of RANK was similar among macrophages cultured on HHA discs, SHA discs, and plastic dishes. Osteoclast precursor cells that strongly expressed RANK and weakly expressed c-Fms dominantly formed osteoclasts *in vivo* rather than osteoclast precursor cells that strongly expressed both RANK and c-Fms [41]. Our results suggest that osteoclast precursor cells strongly expressing RANK and weakly expressing c-Fms are generated on the surface of HA by the suppressed expression of c-Fms, and this may also be associated with the induction of the TRAP-positive MNGCs detected in this study.

In conclusion, our results, which were obtained using the subcutaneous implantation of HA granules, suggest that certain plasma components and the microstructure of HA influence the expression of osteoclast-associated molecules, TRAP and CTSK in MNGCs and functionally divergent MNGCs were inducible in this *in vivo* implantation system.

Acknowledgments

We thank Dr. Kazunori Nakajima for his technical support for the implantation surgery. This work was funded by JSPS KAKENHI (25670834).

References

[1] W.G. Brodbeck, J.M. Anderson, Giant cell formation and function, Curr. Opin. Hematol. 16 (2009) 53–57.
[2] H.K. Vaananen, H. Zhao, M. Mulari, J.M. Halleen, The cell biology of osteoclast function, J. Cell Sci. 113 (Pt. 3) (2000) 377–381.
[3] K. Tezuka, K. Nemoto, Y. Tezuka, T. Sato, Y. Ikeda, M. Kobori, et al., Identification of matrix metalloproteinase 9 in rabbit osteoclasts, J. Biol. Chem. 269 (1994) 15006–15009.
[4] K. Tezuka, Y. Tezuka, A. Maejima, T. Sato, K. Nemoto, H. Kamioka, et al., Molecular cloning of a possible cysteine proteinase predominantly expressed in osteoclasts, J. Biol. Chem. 269 (1994) 1106–1109.
[5] S.M. Krane, M. Inada, Matrix metalloproteinases and bone, Bone 43 (2008) 7–18.
[6] T. Nakayama, T. Mizoguchi, S. Uehara, T. Yamashita, I. Kawahara, Y. Kobayashi, et al., Polarized osteoclasts put marks of tartrate-resistant acid phosphatase on dentin slices – a simple method for identifying polarized osteoclasts, Bone 49 (2011) 1331–1339.
[7] D.L. Lacey, E. Timms, H.L. Tan, M.J. Kelley, C.R. Dunstan, T. Burgess, et al., Osteoprotegerin ligand is a cytokine that regulates osteoclast differentiation and activation, Cell 93 (1998) 165–176.
[8] H. Yasuda, N. Shima, N. Nakagawa, K. Yamaguchi, M. Kinosaki, S. Mochizuki, et al., Osteoclast differentiation factor is a ligand for osteoprotegerin/osteoclastogenesis-inhibitory factor and is identical to TRANCE/RANKL, Proc. Natl. Acad. Sci. U.S.A. 95 (1998) 3597–3602.
[9] T. Nakashima, M. Hayashi, H. Takayanagi, New insights into osteoclastogenic signaling mechanisms, Trends Endocrinol. Metab. 23 (2012) 582–590.
[10] H. Takayanagi, S. Kim, T. Koga, H. Nishina, M. Isshiki, H. Yoshida, et al., Induction and activation of the transcription factor NFATc1 (NFAT2) integrate RANKL signaling in terminal differentiation of osteoclasts, Dev. Cell 3 (2002) 889–901.
[11] M. Asagiri, K. Sato, T. Usami, S. Ochi, H. Nishina, H. Yoshida, et al., Autoamplification of NFATc1 expression determines its essential role in bone homeostasis, J. Exp. Med. 202 (2005) 1261–1269.
[12] M. Yagi, T. Miyamoto, Y. Sawatani, K. Iwamoto, N. Hosogane, N. Fujita, et al., DC-STAMP is essential for cell-cell fusion in osteoclasts and foreign body giant cells, J. Exp. Med. 202 (2005) 345–351.
[13] H. Miyamoto, T. Suzuki, Y. Miyauchi, R. Iwasaki, T. Kobayashi, Y. Sato, et al., Osteoclast stimulatory transmembrane protein and dendritic cell-specific transmembrane protein cooperatively modulate cell-cell fusion to form osteoclasts and foreign body giant cells, J. Bone Miner. Res. 27 (2012) 1289–1297.
[14] A.K. McNally, J.M. Anderson, Foreign body-type multinucleated giant cells induced by interleukin-4 express select lymphocyte co-stimulatory molecules and are phenotypically distinct from osteoclasts and dendritic cells, Exp. Mol. Pathol. 91 (2011) 673–681.
[15] J.M. Anderson, A. Rodriguez, D.T. Chang, Foreign body reaction to biomaterials, Semin. Immunol. 20 (2008) 86–100.
[16] L. Helming, S. Gordon, Molecular mediators of macrophage fusion, Trends Cell Biol. 19 (2009) 514–522.
[17] A.K. McNally, J.M. Anderson, Interleukin-4 induces foreign body giant cells from human monocytes/macrophages. Differential lymphokine regulation of macrophage fusion leads to morphological variants of multinucleated giant cells, Am. J. Pathol. 147 (1995) 1487–1499.
[18] K.M. DeFife, C.R. Jenney, A.K. McNally, E. Colton, J.M. Anderson, Interleukin-13 induces human monocyte/macrophage fusion and macrophage mannose receptor expression, J. Immunol. 158 (1997) 3385–3390.
[19] E. Katsuyama, H. Miyamoto, T. Kobayashi, Y. Sato, W. Hao, H. Kanagawa, et al., Interleukin-1 receptor-associated kinase-4 (IRAK4) promotes inflammatory osteolysis by activating osteoclasts and inhibiting formation of foreign body giant cells, J. Biol. Chem. 290 (2015) 716–726.
[20] S. Wei, M.W. Wang, S.L. Teitelbaum, F.P. Ross, Interleukin-4 reversibly inhibits osteoclastogenesis via inhibition of NF-kappa B and mitogen-activated protein kinase signaling, J. Biol. Chem. 277 (2002) 6622–6630.
[21] Y. Abu-Amer, IL-4 abrogates osteoclastogenesis through STAT6-dependent inhibition of NF-kappaB, J. Clin. Invest. 107 (2001) 1375–1385.
[22] M. Hiasa, M. Abe, A. Nakano, A. Oda, H. Amou, S. Kido, et al., GM-CSF and IL-4 induce dendritic cell differentiation and disrupt osteoclastogenesis through M-CSF receptor shedding by up-regulation of TNF-alpha converting enzyme (TACE), Blood 114 (2009) 4517–4526.
[23] N.C. Stein, C. Kreutzmann, S.P. Zimmermann, U. Niebergall, L. Hellmeyer, C. Goettsch, et al., Interleukin-4 and interleukin-13 stimulate the osteoclast inhibitor osteoprotegerin by human endothelial cells through the STAT6 pathway, J. Bone Miner. Res. 23 (2008) 750–758.
[24] K. Ioku, G. Kawachi, S. Sasaki, H. Fujimori, S. Goto, Hydrothermal preparation of tailrod hyrdoxyapatite, J. Mater. Sci. 41 (2006) 1341–1344.
[25] M. Yoshimura, H. Suda, K. Okamoto, K. Ioku, Hydrothermal synthesis of biocompatible whiskers, J. Mater. Sci. 29 (1994). 3399-2402..
[26] Y. Gonda, K. Ioku, Y. Shibata, T. Okuda, G. Kawachi, M. Kamitakahara, et al., Stimulatory effect of hydrothermally synthesized biodegradable hydroxyapatite granules on osteogenesis and direct association with osteoclasts, Biomaterials 30 (2009) 4390–4400.
[27] T. Okuda, K. Ioku, I. Yonezawa, H. Minagi, Y. Gonda, G. Kawachi, et al., The slow resorption with replacement by bone of a hydrothermally synthesized pure calcium-deficient hydroxyapatite, Biomaterials 29 (2008) 2719–2728.
[28] T. Okuda, K. Ioku, I. Yonezawa, H. Minagi, G. Kawachi, Y. Gonda, et al., The effect of the microstructure of beta-tricalcium phosphate on the metabolism of subsequently formed bone tissue, Biomaterials 28 (2007) 2612–2621.
[29] N.L. Davison, B. ten Harkel, T. Schoenmaker, X. Luo, H. Yuan, V. Everts, et al., Osteoclast resorption of beta-tricalcium phosphate controlled by surface architecture, Biomaterials 35 (2014) 7441–7451.
[30] A.K. McNally, J.M. Anderson, Phenotypic expression in human monocyte-derived interleukin-4-induced foreign body giant cells and macrophages in vitro: dependence on material surface properties, J. Biomed. Mater. Res. A 103 (2015) 1380–1390.
[31] A. Muto, T. Mizoguchi, N. Udagawa, S. Ito, I. Kawahara, Y. Abiko, et al., Lineage-committed osteoclast precursors circulate in blood and settle down into bone, J. Bone Miner. Res. 26 (2011) 2978–2990.
[32] F. Buhling, A. Reisenauer, A. Gerber, S. Kruger, E. Weber, D. Bromme, et al., Cathepsin K – a marker of macrophage differentiation?, J Pathol. 195 (2001) 375–382.
[33] U.A. Khan, S.M. Hashimi, M.M. Bakr, M.R. Forwood, N.A. Morrison, Foreign body giant cells and osteoclasts are TRAP positive, have podosome-belts and

both require OC-STAMP for cell fusion, J. Cell. Biochem. 114 (2013) 1772–1778.
[34] J.K. Park, A. Rosen, J.E. Saffitz, A. Asimaki, S.H. Litovsky, S.M. Mackey-Bojack, et al., Expression of cathepsin K and tartrate-resistant acid phosphatase is not confined to osteoclasts but is a general feature of multinucleated giant cells: systematic analysis, Rheumatology (Oxford) 52 (2013) 1529–1533.
[35] B. Ten Harkel, T. Schoenmaker, D.I. Picavet, N.L. Davison, T.J. de Vries, V. Everts, The foreign body giant cell cannot resorb bone, but dissolves hydroxyapatite like osteoclasts, PLoS ONE 10 (2015). e0139564.
[36] T. Ikeda, M. Kasai, E. Tatsukawa, M. Kamitakahara, Y. Shibata, T. Yokoi, et al., A bone substitute with high affinity for vitamin D-binding protein-relationship with niche of osteoclasts, J. Cell. Mol. Med. 18 (2014) 170–180.
[37] E. Tatsukawa, Y. Gonda, M. Kamitakahara, M. Matsuura, M. Ushijima, Y. Shibata, et al., Promotion of normal healing of bone defects under estrogen deficiency by implantation of beta-tricalcium phosphate composed of rod-shaped particles, J. Orthop. Res. 32 (2014) 189–196.
[38] T. Albrektsson, C. Dahlin, T. Jemt, L. Sennerby, A. Turri, A. Wennerberg, Is marginal bone loss around oral implants the result of a provoked foreign body reaction?, Clin Implant Dent. Relat. Res. 16 (2014) 155–165.
[39] R. Trindade, T. Albrektsson, P. Tengvall, A. Wennerberg, Foreign body reaction to biomaterials: on mechanisms for buildup and breakdown of osseointegration, Clin. Implant Dent. Relat. Res. 18 (2016) 192–203.
[40] J. Kzhyshkowska, A. Gudima, V. Riabov, C. Dollinger, P. Lavalle, N.E. Vrana, Macrophage responses to implants: prospects for personalized medicine, J. Leukoc. Biol. 98 (2015) 953–962.
[41] T. Mizoguchi, A. Muto, N. Udagawa, A. Arai, T. Yamashita, A. Hosoya, et al., Identification of cell cycle-arrested quiescent osteoclast precursors in vivo, J. Cell Biol. 184 (2009) 541–554.